INSTITUTE OF PHYSICS PUBLISHING PLASMA SOURCES SCIENCE AND TECHNOLOGY
Plasma Sources Sci. Technol. **13** (2004) 8–14 PII: S0963-0252(04)67711-5

Plasma enhanced chemical vapour deposition of hydrogenated amorphous silicon at atmospheric pressure

M Moravej[1], S E Babayan[2], G R Nowling[1], X Yang[1] and R F Hicks[1]

[1] Chemical Engineering Department, University of California, Los Angeles, CA 90095, USA
[2] Surfx Technologies LLC, 10624 Rochester Ave., Los Angeles, CA 90024, USA

E-mail: rhicks@ucla.edu

Received 10 January 2003, in final form 13 August 2003
Published 11 November 2003
Online at stacks.iop.org/PSST/13/8 (DOI: 10.1088/0963-0252/13/1/002)

Abstract
Amorphous hydrogenated silicon films were grown using an atmospheric pressure helium and hydrogen plasma with silane added downstream of the source. A maximum deposition rate of 120 ± 12 Å min^{-1} was recorded at a substrate temperature of 450°C, 6.3 Torr H_2, 0.3 Torr SiH_4, 778 Torr He, 32.8 W cm^{-3}, and an electrode-to-substrate spacing of 6.0 mm. The deposition rate increased rapidly with the silane and hydrogen partial pressures, up to 0.1 and 7.0 Torr, respectively, then remained constant thereafter. By contrast, the deposition rate decreased exponentially as the electrode-to-substrate distance was increased from 5.0 to 10.5 mm. The total hydrogen content of the films ranged from 2.5 to 8.0 ± 1.0 at%. These results together with a model of the plasma chemistry indicate that H atoms and SiH_3 radicals play an important role in the deposition process.

1. Introduction

Amorphous hydrogenated silicon is widely used in solar cells and thin film transistors (TFT) for flat panel displays [1–10]. This material is normally grown on glass substrates at temperatures below 500°C by plasma enhanced chemical vapour deposition (PECVD). Radio-frequency capacitive discharges are often used for this process, although inductively coupled plasmas (ICP), electron cyclotron resonance (ECR) sources, and helicon waves have been explored for this purpose as well [1–4, 11]. Capacitive discharges exhibit electron densities in the range 10^9–10^{11} cm^{-3} with average electron temperatures near 3.0 eV. By contrast, ICP, ECR, and helicon wave sources generate higher electron densities, between 10^{10} and 10^{13} cm^{-3}, but are more difficult to design and operate for large-area PECVD applications [11].

We have developed an atmospheric pressure plasma that exhibits physical and chemical characteristics similar to low-pressure discharges [12–18]. The plasma is generated by flowing helium and a reactive gas between two closely spaced metal electrodes, in which one of the electrodes is connected to a radio frequency power source. The discharge is capacitive and is sustained by bulk ionization of the gas suspended between the sheaths. For a pure helium atmospheric pressure plasma, we have measured an electron density of 3.0×10^{11} cm^{-3}, an average electron temperature of 2.0 eV, and a neutral temperature of 120°C [12, 13]. Recently, it has been shown that this plasma source may be scaled up to uniformly treat large substrate areas [19]. The high-pressure operation combined with the reasonably high electron density suggests that this gas discharge may have certain advantages for materials processing.

In this paper, we examine the deposition of amorphous hydrogenated silicon using an atmospheric pressure helium and hydrogen plasma with downstream addition of silane. The effect of the process variables on the a-Si : H deposition rate and hydrogen content in the films has been determined. In addition, a numerical model of the plasma chemistry has been developed to identify which reactive species are likely to be involved in the deposition process. A comparison of the model results with the experimental data indicates that ground-state hydrogen atoms and SiH_3 radicals are the most abundant reactive intermediates.

2. Experimental methods

A schematic of the plasma source used in the PECVD experiments is shown in figure 1. The source consisted of two aluminium electrodes, 33 mm in diameter, separated by a gap 1.6 mm wide. Both electrodes were perforated to allow helium and hydrogen to flow through them. The upper electrode was connected to a radio frequency power supply (13.56 MHz), while the lower electrode was grounded. A third aluminium plate was installed beneath the lower electrode. It contained an internal network of channels and holes that mixed silane with the plasma afterglow. Located 5.0–10.5 mm further downstream was a rotating sample stage and heater, both with adjustable heights.

The films were deposited by the following procedure: a Corning 1737 glass substrate was rinsed with acetone and methanol, and placed on the sample holder. Then, helium and hydrogen were fed to the plasma source at flow rates of 40.0 l min^{-1} and 0.0–920 cm^3 min^{-1}, respectively. After a 10 min purge, the sample was heated to a temperature between 100˚C and 450˚C, and the discharge ignited with 45 W of RF power. Then, after one additional minute, the PECVD reaction was started by feeding 5.0% SiH_4 in He at 0.31–48.0 cm^3 min^{-1}. Growth was carried out for 10 min, after which the silane flow was stopped, and 1 min later the plasma was extinguished. All the runs were performed at 32.8 W cm^{-3} (45 W), 778 Torr helium, and a rotation rate of 200 rpm. Periodically, to check the reproducibility of the process, the films were deposited at 300˚C, 6.3 Torr H_2, 0.3 Torr SiH_4, and an electrode-to-substrate distance of 6.0 mm. At these standard conditions, the growth rate was 62.0 ± 5.0 Å min^{-1}.

The thickness of the films was measured with a Tencor Alpha-Step 200. A step was created by first protecting half of the film with a silicone sealant (GE Translucent RTV 108). Then, the unmasked region was etched in heated potassium hydroxide solution. After etching, the silicon sealant was removed by rinsing it with acetone and methylethylketone. The uniformity across the deposited region in several films was found to be 3.2% of 1σ, and was determined by taking the standard deviation of 30 points across the substrate. For each sample, the thickness reported is an average of five points taken along the substrate. To calculate the deposition rate, the measured thickness was divided by the 10 min reaction time. In separate experiments, it was confirmed that the rate remained constant over a 0–30 min growth period.

The hydrogen composition in the films was analysed by infrared spectroscopy, using a Bio-Rad FTS-40A with a DTGS detector. For these measurements, the hydrogenated amorphous silicon films were deposited on gallium arsenide internal reflection elements that were 4.0 cm long by 1.0 cm wide by 0.6 cm thick with 45˚ bevelled edges. The beam passing through the crystal reflected 37 times off the front face that was coated with the film. The spectra were collected at a resolution of 4 cm^{-1} and signal-averaging 512 scans. The infrared absorbance spectrum was obtained by taking the ratio of the single-beam spectrum of the wafer and the film minus that of the blank wafer. The hydrogen content in one film was analysed by hydrogen forward scattering using a 2.275 MeV He^{2+} ion beam with a detector angle of 30˚. The structure of one of the samples was determined by Raman spectroscopy with a 514.5 nm Ar^+ laser.

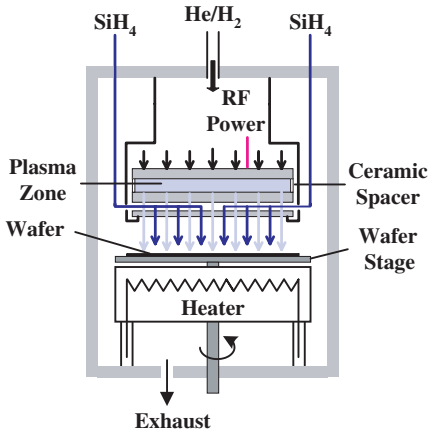

Figure 1. Schematic of the atmospheric pressure PECVD chamber.

3. Results

3.1. Trends in growth rate

In figure 2, we show the dependence of the growth rate on the substrate temperature. The temperature was varied from 100˚C to 450˚C, while holding the H_2 and SiH_4 partial pressures constant at 6.3 Torr and 0.3 Torr, respectively. The temperature in the plasma afterglow was 100˚C, which established the lower limit for this experiment. As can be seen in figure 2, the growth rate increases linearly with substrate temperature, from 70 to 120 Å min^{-1}. The etch rate of the films (with KOH) was estimated to determine if the density of the films change with substrate temperature. The etch rate varied by less than 10% between the 100˚C and 450˚C samples. This constant rate indicates that the density of the films did not change appreciably with temperature and, therefore, the deposition rate was not corrected for the density.

The dependence of the deposition rate on the electrode-to-substrate distance is shown in figure 3. The other conditions were 300˚C, 6.3 Torr H_2 and 0.3 Torr SiH_4. The rate decreases exponentially from 92 to 13 Å min^{-1} as the distance increases from 5.0 to 10.5 mm. Evidently, the reactive species that are responsible for film growth rapidly decrease in concentration as they move downstream away from the plasma source.

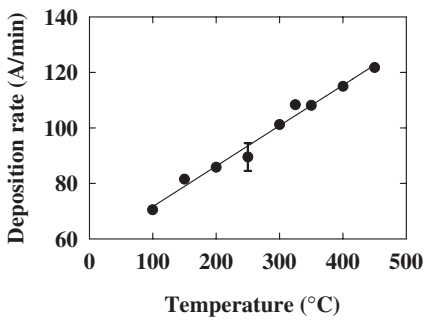

Figure 2. The dependence of the deposition rate on substrate temperature.

In figure 4 we present the dependence of the a-Si : H growth rate on the H_2 partial pressure. The conditions were 300°C, 0.3 Torr SiH_4, and an electrode-to-substrate distance of 6.0 mm. Note that deposition does not occur unless hydrogen is added to the plasma. The growth rate increases from 0.0 to 65.0 Å min^{-1} as the hydrogen pressure increases from 0.0 to 7.0 Torr. Thereafter, the rate remains constant as the H_2 pressure is raised to 18.0 Torr. These data show that the hydrogen plasma produces reactive intermediates (i.e. H atoms) that are required to drive the PECVD process. Above about 7.0 Torr H_2, these intermediates are no longer the limiting reagent.

In figure 5 we show the dependence of the a-Si : H growth rate on the SiH_4 partial pressure at 300°C, 6.3 Torr H_2 and a spacing of 6.0 mm. Initially, the rate increases rapidly as the silane pressure is raised from 0.0 to 0.1 Torr. Then, it stays constant at 62.0 Å min^{-1} with further increases in SiH_4 pressure. These results suggest that silane is the limiting reagent for a-Si : H deposition below 0.1 Torr, but is present in excess quantity at higher pressures.

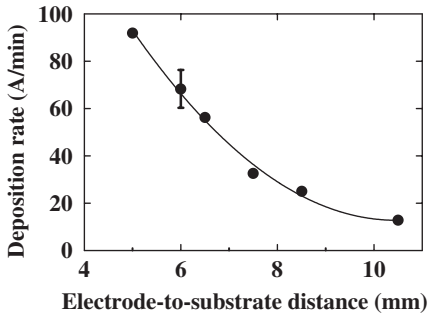

Figure 3. The dependence of the deposition rate on electrode-to-substrate distance.

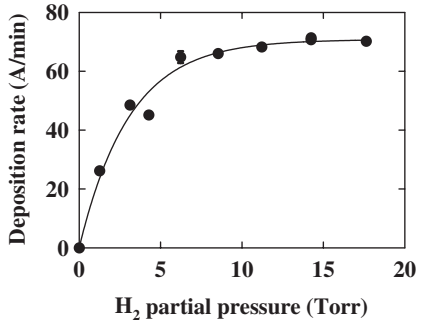

Figure 4. The dependence of the deposition rate on the H_2 partial pressure.

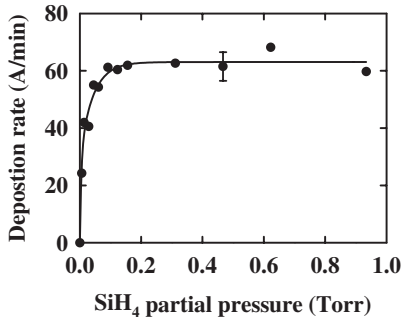

Figure 5. The dependence of the deposition rate on the SiH_4 partial pressure.

3.2. Film properties

The hydrogen content in the films was determined as a function of the H_2 partial pressure and the substrate temperature. In figure 6 we show the infrared reflectance spectrum of the Si–H stretching region for an a-Si : H film deposited at 300°C, 6.3 Torr H_2, 0.3 Torr SiH_4, and an electrode-to-substrate distance of 6.0 mm. Deposition occurred for 20 min, yielding a thickness of 1400 Å. After deconvolution of the spectrum, three peaks are obtained at 2003, 2080, and 2120 cm^{-1}. The peak at 2003 cm^{-1} is attributed to silicon monohydride stretching vibrations, whereas the peak at 2120 cm^{-1} is due to the asymmetric stretching mode of SiH_2 groups [20, 21]. The feature at 2080 cm^{-1} may be due to the stretching vibrations of silicon hydride clusters, or to the symmetric stretching mode of SiH_2 groups [9, 10, 22–25].

The concentration of the SiH and SiH_2 species were calculated from the integrated area under the peaks at 2003 and 2120 cm^{-1}, using their known absorption coefficients. These coefficients are 1.11×10^{-20} and 4.55×10^{-21} cm^2 per oscillator, respectively [26, 27]. The peak at 2080 cm^{-1} was not included in the H content calculations because it can be either due to SiH_2 stretching or SiH clusters, whose concentrations were calculated from the other two peaks. The hydrogen content of a film grown at 100°C was determined by hydrogen forward scattering as well as by vibrational spectroscopy. The HFS measurement yielded a value of 6.5 at% compared to 5.5 at% from the infrared absorbance.

The microstructure parameter, R^*, which is defined as the ratio of the integrated area of the peaks at 2120 and 2080 cm^{-1} to the sum of all three peaks, was determined from the IR spectra. This value is 0.35 for the data shown in figure 6. The R^* parameter gives an indication of the fraction of H that is bonded in the dihydride form and to internal surfaces of voids, versus that bonded in the monohydride form [28–31]. It ranges from 0 to 1 and the closer it is to 0, the less voids and the denser the film [31]. Films with values less than 0.1 exhibit carrier mobilities that are suitable for use in photovoltaic devices [32, 33]. The Raman spectra of a sample deposited at 6.3 Torr H_2, 0.3 Torr SiH_4, and 450°C showed only one peak at ∼480 cm^{-1}, indicating that the film was amorphous.

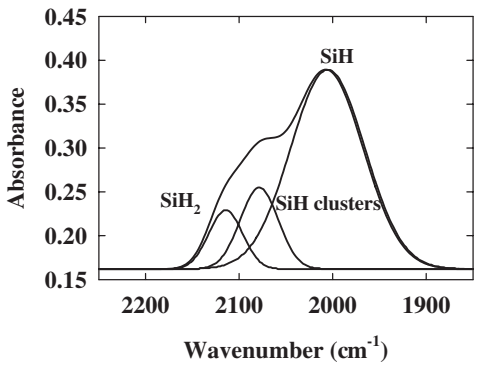

Figure 6. Infrared spectra of an a-Si : H film deposited on a GaAs crystal.

The dependence of the hydrogen content on the H_2 pressure is shown in figure 7. The conditions were 300°C, 0.3 Torr SiH_4, and an electrode-to-substrate distance of 6.0 mm. The total hydrogen concentration decreases from 8.0 to 5.0 ± 1.0 at% as the H_2 pressure rises from 4.3 to 17.6 Torr. The silicon monohydride species follows a similar trend, decreasing in concentration from 5.5 to 3.0 at%. In contrast, the silicon dihydride species stays constant at 2.0 at%. At the higher hydrogen pressures, approximately three quarters of the total hydrogen is in the monohydride form. The microstructure parameter remains constant at 0.3 ± 0.1 as the hydrogen partial pressure increases from 4.3 to 17.6 Torr.

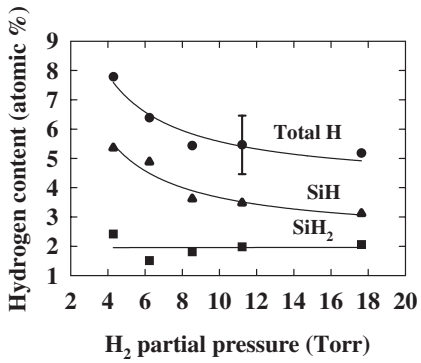

Figure 7. The hydrogen concentration in the a-Si : H films as a function of the H_2 partial pressure.

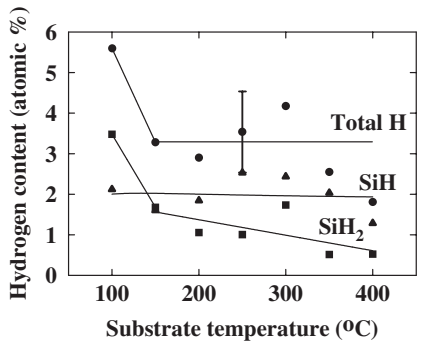

Figure 8. The hydrogen concentration in the a-Si : H films as a function of the substrate temperature.

The dependence of the hydrogen content on the substrate temperature is shown in figure 8. The amount of hydrogen incorporated into the films declines from 6.0 to 3.0 ± 1.0 at% as the temperature rises from 100 to 150°C; thereafter it remains constant at ∼3.0 at%. The total amount of H present as silicon monohydride increases with temperature as well, from 36% at 100°C to 90% at 400°C. The microstructure parameter decreases from 0.7 to 0.3 ± 0.1 as the temperature increases from 100°C to 150°C; thereafter, it remains constant at $\sim 0.3 \pm 0.1$ up to 400°C. This implies that the films grown at 100°C contain a much higher density of voids compared to films grown at 150°C and above.

3.3. Model of the plasma chemistry

A one-dimensional 'plug-flow' model has been developed to investigate the reaction chemistry in the plasma and the afterglow [16]. In the model it was assumed that the process is at steady state, and the gas is perfectly mixed in the cross-flow direction, but unmixed in the flow direction. The reactions used in these simulations are listed in table 1. In the discharge region, only reactions 1 and 2 are needed, since no silane is present there. On the other hand, in the afterglow, one may assume that the electron and ion concentrations are negligible, so that this portion of the process may be modelled with reactions 2–20 [12, 16]. The rate constant for reaction 2 in table 1 has been changed to a pseudo-bimolecular rate by

Table 1. Gas phase reactions used in the model.

	Reaction	Rate constant at 373 K ($cm^3\ s^{-1}$)	Reference
1[a]	$H_2 + e^- \rightarrow H + H + e^-$	$5.7 \times 10^{-9}(T_e^{0.069}) \exp(-8.5 \times 10^4/T_e)$	[34–36]
2	$H + H + He \rightarrow H_2 + He$	1.4×10^{-13}	[37]
3	$H + SiH_4 \rightarrow SiH_3 + H_2$	2.0×10^{-12}	[38]
4	$H + SiH_3 \rightarrow SiH_2 + H_2$	1.0×10^{-10}	[35]
5	$H + SiH_2 \rightarrow SiH + H_2$	3.3×10^{-10}	[40]
6	$SiH_3 + SiH_3 \rightarrow SiH_2 + SiH_4$	7.0×10^{-12}	[39]
7	$SiH_2 + H_2 \rightarrow SiH_4$	3.0×10^{-12}	[40]
8	$SiH_2 + H \rightarrow SiH_3$	2.3×10^{-11}	[39]
9	$SiH + H_2 \rightarrow SiH_3$	2.0×10^{-12}	[39]
10	$SiH_2 + SiH_4 \rightarrow Si_2H_6$	1.0×10^{-11}	[39]
11	$SiH_3 + SiH_3 \rightarrow Si_2H_6$	1.0×10^{-11}	[39]
12	$SiH_2 + Si_2H_6 \rightarrow Si_3H_8$	3.9×10^{-10}	[40]
13	$H + Si_2H_6 \rightarrow SiH_3 + SiH_4$	2.9×10^{-13}	[40]
14	$H + Si_2H_6 \rightarrow Si_2H_5 + H_2$	5.5×10^{-12}	[40]
15	$H + Si_3H_8 \rightarrow Si_2H_5 + SiH_4$	8.4×10^{-12}	[40]
16	$SiH + SiH_4 \rightarrow H_2 + Si_2H_3$	4.4×10^{-10}	[40]
17	$SiH_3 + Si_2H_6 \rightarrow Si_2H_5 + SiH_4$	5.0×10^{-13}	[40]
18	$SiH_3 + Si_2H_5 \rightarrow Si_2H_4 + SiH_4$	1.0×10^{-10}	[41]
19	$H + Si_2H_5 \rightarrow Si_2H_4 + H_2$	1.0×10^{-10}	[41]
20	$SiH_3 + Si_3H_8 \rightarrow Si_4H_9 + H_2$	1.0×10^{-11}	[39]

[a] T_e is in K.
Reactions 2 and 7–12 are three-body reactions with the concentration of the third body already accounted for in the constant.

multiplying the termolecular rate with the concentration of He present in the system. The rates for reactions 7–12 have also been changed to bimolecular rates in the references they were obtained from. In these simulations, the gas temperature was assumed to be constant at 100°C.

In order to calculate the rate of electron impact dissociation of H_2, reaction 1, one needs to know the electron density, n_e, and temperature, T_e. These parameters may be estimated for the atmospheric pressure plasma using the procedure given by Park *et al* [13, 14]. For an alpha-mode capacitive discharge, the current density, J, depends on the bulk electric field strength, E, as follows:

$$J = -n_e e \mu_e E, \tag{1}$$

where e is a unit of electron charge, and μ_e is the electron mobility, equal to $1.7 \times 10^3\ \mathrm{cm^2\ V^{-1} s^{-1}}$ at 780 Torr [11]. The discharge voltage and current for the plasma was measured with an advanced energy impedance probe (RFZ 60). At the standard process conditions, these parameters were 225 V and 3.25 A, yielding a current density of $0.38\ \mathrm{A\ cm^{-2}}$ and an electric field of $1406\ \mathrm{V\ cm^{-1}}$. Based on these values, the plasma density was calculated to be $1.0 \times 10^{12}\ \mathrm{cm^{-3}}$.

The electron temperature may be estimated from a power balance, which assumes that the plasma energy is dissipated by electron heating of the gas [13]:

$$P_{in} \approx n_e \left(\frac{3}{2} k T_e - \frac{3}{2} k T_n\right) 2 \left(\frac{m_e}{m_{He}}\right) \nu_{en}. \tag{2}$$

Here, P_{in} is the input power, k is the Boltzmann constant, T_n is the neutral temperature, m_e is the mass of an electron, m_{He} is the mass of a helium atom, and ν_{en} is the electron–neutral collision frequency. Using this equation and the value of n_e already calculated, a T_e of 1.0 eV is obtained. For an electron density and temperature of $1.0 \times 10^{12}\ \mathrm{cm^{-3}}$ and 1.0 eV, the pseudo-first-order rate constant for electron impact dissociation of H_2 is $6.9 \times 10^{-12}\ \mathrm{cm^3\ s^{-1}}$.

The simulation was carried out in two parts. First, the H atom concentration in the discharge was calculated given an H_2 feed concentration of $2.0 \times 10^{17}\ \mathrm{cm^{-3}}$ (6.2 Torr). Then, the species profiles in the afterglow were calculated for an SiH_4 feed concentration of $8.0 \times 10^{14}\ \mathrm{cm^{-3}}$, and the H atom concentration obtained from the previous model. Based on a two-dimensional numerical model of the hydrodynamics in the showerhead, it was concluded that only 10% of the silane mixed with the plasma stream. For this reason, a concentration of $8.0 \times 10^{14}\ \mathrm{cm^{-3}}$ was used in the simulation corresponding to an SiH_4 feed pressure of 0.03 Torr (10% of the actual value).

The design of the perforated electrodes was such that the gas was well mixed in the plasma zone. Consequently, the residence time in the plasma equalled the volume between the electrodes divided by the volumetric flow rate, i.e. 2 ms. The relationship between the time and distance downstream of the electrodes is more complicated than in the plasma zone. The gas emerges as a series of laminar flowing jets. The velocity of the fluid in the jet varies from the centre to the edge, and as it travels downstream due to radial expansion. Simulations of the fluid dynamics were performed using a CFD software package (FEMLAB). It was found that the average velocity in the jet 1, 3 and 6 mm below the bottom electrode, at the standard process conditions, was $13.2\ \mathrm{m\ s^{-1}}$, $10.3\ \mathrm{m\ s^{-1}}$, and $8.5\ \mathrm{m\ s^{-1}}$, respectively. Therefore, an overall average gas velocity of $10.0\ \mathrm{m\ s^{-1}}$ was assumed.

In figure 9 we present the species profiles predicted from the numerical model. The shaded region from 0 to 2 ms represents the plasma, while the unshaded region from 2 to 4 ms represents the afterglow. According to the model, the hydrogen atom density is a maximum, equal to $2.6 \times 10^{15}\ \mathrm{cm^{-3}}$, at the end of the discharge. Then, this species is rapidly consumed by reaction with silane to produce SiH_3 radicals and H_2. After 2 ms, the concentration of H atoms in the afterglow falls to about $2.0 \times 10^{13}\ \mathrm{cm^{-3}}$. The products of the H atom reaction with silane are disilane and the silyl radicals, SiH_3, SiH_2, and SiH. The latter three species attain maximum concentrations of 3.0×10^{13}, 5.0×10^{12}, and $5.0 \times 10^{12}\ \mathrm{cm^{-3}}$ just beyond the leading edge of the afterglow. Thereafter, the SiH_2 and SiH species decay rapidly due to reaction with H_2 (steps 7 and 9 in table 1). On the other hand, the concentration of SiH_3 declines more slowly through binary recombination reactions 4, 6, 17, 18, 20, and the termolecular reaction 11. The rate constant for the reverse of reaction 3 was calculated, using thermodynamic data, to be $\sim 1.0 \times 10^{-19}\ \mathrm{cm^3\ s^{-1}}$. This rate is too slow to affect the consumption rate of SiH_3 radicals in the downstream region. The six consumption reactions for SiH_3 all involve collisions between two species present in low concentration, $<10^{15}\ \mathrm{cm^{-3}}$, consequently, the SiH_3 concentration falls off slowly from 2.5 to 4.0 ms in the afterglow. Given that the substrate is located between 5.0 and 10.5 mm downstream, the simulation indicates that H and SiH_3 are the dominant reactive intermediates present in the gas immediately above the growing film [41–47].

The numerical model was used to investigate the dependence of the SiH_3 concentration in the afterglow on the SiH_4 pressure in the feed. These results are shown in figure 10 for the SiH_3 concentration calculated 6 mm below the bottom electrode (equivalent to an afterglow reaction time of 0.6 ms). Note that only 10% of the SiH_4 feed pressure was input into the simulations to account for the inefficient mixing in the real system. One sees that the silyl radical density quickly rises to about $1.5 \times 10^{13}\ \mathrm{cm^{-3}}$ at 0.1 Torr SiH_4, and thereafter remains constant as the silane pressure increases further. The knee in the curve corresponds to the 'titration point', where the concentration of SiH_4 equals that

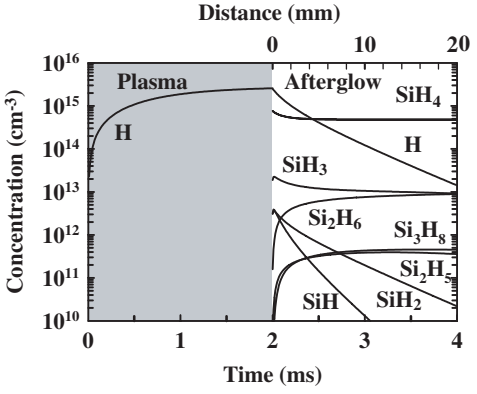

Figure 9. The predicted concentrations of the species in the plasma and the afterglow as a function of time and distance.

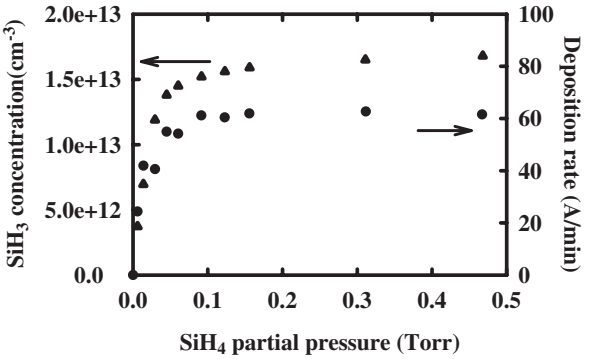

Figure 10. The dependence of the predicted SiH_3 concentration and the observed deposition rate on the SiH_4 partial pressure.

of the H atoms. A pressure of 0.02 Torr yields a molecular density of 2.1×10^{15} cm^{-3}, compared to the calculated H atom concentration of 2.6×10^{15} cm^{-3}.

In figure 10, we show the observed dependence of the deposition rate on the silane pressure, so that it may be compared directly to the simulations. The trend in the deposition rate closely follows that exhibited by the SiH_3 concentration. Based on these results, one may surmise that H atoms and SiH_3 radicals are important reactive intermediates in the PECVD process, and that the concentration of H atoms produced by the helium-stabilized, atmospheric pressure plasma is in the range of $2.0 \pm 1.5 \times 10^{15}$ cm^{-3}.

4. Discussion

The gas-phase radical reaction chemistry presented in table 1 can explain in a qualitative way the influence of the process conditions on the PECVD deposition rate and the hydrogen content in the films. Electron impact dissociation of hydrogen molecules in the plasma produces $\sim 10^{15}$ cm^{-3} ground-state hydrogen atoms. It should be noted that this density is in the same range as the densities of O or N atoms generated by the helium-stabilized atmospheric pressure plasma when O_2 or N_2 is substituted for H_2 in the feed [15, 16]. The ground-state hydrogen atoms emerge from the discharge and mix with silane, where they react with it to form SiH_3, and to a lesser extent, SiH_2 and SiH. The growth rate is proportional to the flux of SiH_3 to the substrate (as shown in figure 10). The dependence of the deposition rate on the hydrogen pressure (cf figure 4) has a similar explanation. For an SiH_4 feed pressure of 0.3 Torr, the H atoms limit the conversion of SiH_4 to SiH_3 below an H_2 partial pressure of about 8.0 Torr. At lower H_2 pressures, less SiH_3 is produced, hence the deposition rate decreases. Above 8.0 Torr H_2, SiH_4 becomes the limiting reagent, and no change in growth rate is seen. The exponential decay in the deposition rate with electrode-to-substrate spacing (cf figure 3) is harder to explain, but could be related to the rapid fall off in the density of the H radicals with distance in the afterglow.

In order to understand how the process conditions influence the hydrogen content in the film, one must combine the gas-phase chemistry with the surface reactions that result in a-Si : H deposition. According to the literature [43–49], some fraction of the SiH_3 radicals adsorb on to the film surface and become part of an active SiH_x layer. Then, silyl radicals impinge on the adsorbed SiH_x abstracting H atoms, and causing the surface silicon to be incorporated into the film. According to figure 7, the H content in the film is unchanged above 8.0 Torr H_2, whereas it increases with decreasing H_2 pressure below this point. The 8.0 Torr value corresponds to the transition point from H-atom to SiH_4 limited growth. Above 8.0 Torr the flux of silyl radicals to the surface is constant, so that the abstraction rate and in turn the H content of the film is unchanged. Below 8.0 Torr, the SiH_3 flux to the surface decreases with decreasing H_2 pressure, leading to an increase in the H content of the film.

In the following paragraph we present a comparison between the atmospheric pressure and low-pressure PECVD of amorphous hydrogenated silicon. Our attention is restricted to remote systems where the substrate is located downstream of the plasma, and there is no ion bombardment. A deposition rate of 5 Å min^{-1} was obtained with an ICP source at 0.2 Torr pressure, 200°C substrate temperature, and the silane plus hydrogen added to the plasma [20]. On the other hand, a maximum growth rate of 35 Å min^{-1} was observed with an ICP hydrogen–helium plasma at 0.3 Torr pressure, 200°C, and the silane added downstream [50]. These results may be compared to this study, where a deposition rate of 65 Å min^{-1} was recorded at atmospheric pressure and 200°C. It should be noted that rates as high as 6000 Å min^{-1} have been achieved with an expanding thermal plasma (cascaded arc), which although a remote system, has a high density of ionic and thermally activated species that can be involved in the gas phase reactions [51].

A further difference between low-pressure and atmospheric pressure PECVD is the hydrogen content in the films. We recorded values ranging from 3.0 to 6.0 at% H. This may be compared to hydrogen contents of 7.0–15.0 at% in remote low-pressure PECVD reactors [21, 22, 27, 49, 52–56]. This is most probably related to the higher concentration of radicals produced in the atmospheric pressure discharge, e.g. 10^{15} cm^{-3} of H atoms and 10^{13} cm^{-3} of SiH_3 [57–59]. The increased radical pool should lead to higher abstraction rates of hydrogen from the film surface [60–62].

5. Conclusions

We have examined the deposition of amorphous hydrogenated silicon films using a low-temperature, atmospheric pressure hydrogen plasma with downstream injection of silane. It is concluded that H atoms and SiH_3 radicals are the principal reactive intermediates involved in film growth. The low hydrogen content in the films, ~3.0 at%, attests to the high radical density in the atmospheric pressure plasma. Nevertheless, deposition rates are relatively low in this process, ranging from 70 Å min^{-1} at 100°C to 120 Å min^{-1} at 450°C.

Acknowledgments

This work was supported by grants from the US Department of Energy, Environmental Management Sciences Program, the University of California SMART program, and AMD.

References

[1] Luft W and Tsuo Y S 1993 *Hydrogenated Amorphous Silicon Alloy Deposition Processes* (New York: Dekker)
[2] Bruno G, Capezzuto P and Madan A 1995 *Plasma Deposition of Amorphous Silicon-Based Materials* (New York: Academic)
[3] Konuma M 1998 *Film Deposition by Plasma Techniques* (Berlin: Springer)
[4] Street R A 2000 *Technology and Applications of Amorphous Silicon* (Berlin: Springer)
[5] Bneking C, Rech B, Wieder S, Kluth O, Wagner H, Frammelsberger W, Geyer R, Lechner P, Rübel H and Schade H 1999 *Thin Solid Films* **351** 241
[6] Takeuchi Y, Nawata Y, Ogawa K, Serizawa A, Yamauchi Y and Murata M 2001 *Thin Solid Films* **386** 133
[7] Kondo M and Matsuda A 2001 *Thin Solid Films* **383** 1
[8] Lihui G and Rongming L 2000 *Thin Solid Films* **376** 249
[9] Marra D C, Edelberg E A, Naone R L and Aydil E S 1998 *J. Vac. Sci. Technol.* A **16** 3199
[10] Marra D C, Edelberg E A, Naone R L and Aydil E S 1998 *Appl. Surf. Sci.* **133** 148
[11] Lieberman M A and Lichtenberg A J 1994 *Principles of Plasma Discharges and Materials Processing* (New York: Wiley)
[12] Schütze A, Jeong J Y, Babayan S E, Park J, Selwyn G S and Hicks R F 1998 *IEEE Trans. Plasma Sci.* **26** 1685
[13] Park J, Henins I, Herrmann H W, Selwyn G S and Hicks R F 2001 *J. Appl. Phys.* **89** 20
[14] Park J, Henins I, Herrmann H W and Selwyn G S 2000 *Phys. Plasmas* **7** 3141
[15] Babayan S E, Ding G and Hicks R F 2001 *Plasma Chem. Plasma Process.* **21** 505
[16] Jeong J Y, Park J, Henins I, Babayan S E, Tu V J, Selwyn G S, Ding G and Hicks R F 2000 *J. Phys. Chem.* **104** 8027
[17] Nowling G R, Babayan S E, Jankovic V and Hicks R F 2002 *Plasma Sources Sci. Technol.* **11** 97
[18] Babayan S E, Jeong J Y, Schütze A, Tu V J, Moravej M, Selwyn G S and Hicks R F 2001 *Plasma Sources Sci. Technol.* **10** 573
[19] www.surfxtechnologies.com
[20] Anthony B, Hsu T, Breaux L, Qian R, Banerjee S and Tasch A 1990 *J. Electron. Mater*. **19** 1089
[21] Lee J N, Lee B J, Moon D G and Ahn B T 1997 *Japan. J. Appl. Phys.* **36** 6862
[22] Sidhu L S and Zukotynski S 1999 *J. Non-Cryst. Solids* **246** 65
[23] Lucovsky G, Nemanich R J and Knights J C 1979 *Phys. Rev.* B **19** 2064
[24] Katiyar M and Abelson J R 2001 *Mater. Sci. Engng.* A **304–306** 349
[25] Katiyar M, Feng G F, Yang Y H, Abelson J R and Maley N 1993 *Appl. Phys. Lett.* **63** 461
[26] Langford A A, Fleet M L, Nelson B P, Lanford W A and Maley N 1992 *Phys. Rev.* B **45** 367
[27] Severens R J, Brussaard G J H, van de Sanden M C M and Schram D C 1995 *Appl. Phys. Lett.* **67** 491
[28] Biebericher A C W, van der Weg W F and Rath J K 2003 *J. Vac. Sci. Technol.* A **21** 156
[29] Lenski M and Comes F J 1996 *Thin Solid Films* **288** 337
[30] Schmidt J A, Koropecki R R, Arce R and Buitrago R H 1995 *J. Appl. Phys.* **78** 5959
[31] Desalvo A, Giorgis F, Pirri C F, Tresso E, Rava P, Galloni R, Rizzoli R and Summonte C 1997 *J. Appl. Phys*. **81** 7973
[32] Guha S, Yang J, Jones S J, Chen Y and Williamson D L 1992 *Appl. Phys. Lett.* **61** 1444
[33] Biebericher A C W, van der Weg W F, Rath J K, Akdim M R and Goedheer W J 2002 *J. Vac. Sci. Technol.* A **21** 156
[34] Trevisan C S and Tennyson J 2002 *Plasma Phys. Control Fusion* **44** 1263
[35] Beuthe T G and Chang J S 1999 *Japan. J. Appl. Phys.* **38** 4576
[36] Meeks E, Larson R S, Ho P, Apblett C, Han S M, Edelberg E and Aydil E S 1998 *J. Vac. Sci. Technol.* A **16** 544
[37] Goumri A, Yuan W J, Ding L, Shi Y and Marshall P 1993 *Chem. Phys.* **177** 233
[38] Kushner M J 1988 *J. Appl. Phys.* **63** 2532
[39] Leroy O, Gousset G, Alves L L, Perrin J and Jolly J 1998 *Plasma Sources Sci. Technol.* **7** 348
[40] Perrin J 1993 *J. Phys. D: Appl. Phys.* **26** 1662
[41] Longeway P A, Weakliem H A and Estes R D 1984 *J. Phys. Chem.* **88** 3282
[42] Longeway P A, Estes R D and Weakliem H A 1984 *J. Phys. Chem.* **88** 73
[43] Kessels W M M, Hoefnagels J P M, Boogaarts M G H, Schram D C and van de Sanden M C M 2001 *J. Appl. Phys.* **89** 2065
[44] Robertson J 2000 *J. Appl. Phys.* **87** 2608
[45] Matsuda A 1999 *Thin Solid Films* **337** 1
[46] Robertson R and Gallagher A 1986 *J. Chem. Phys.* **85** 3623
[47] Kessels W M M, Smets A H M, Marra D C, Aydil E S, Schram D C and van de Sanden M C M 2001 *Thin Solid Films* **383** 154
[48] Gerbi J E and Abelson J R 2001 *J. Appl. Phys.* **89** 1463
[49] Srinivasan E, Lloyd D A and Parsons G N 1997 *J. Vac. Sci. Technol.* A **15** 77
[50] Lee S W, Heo D C, Kang J K, Park Y B and Rhee S W 1998 *J. Electrochem. Soc.* **145** 2900
[51] Kessels W M M, Severens R J, Smets A H M, Korevaar B A, Adriaenssens G J, Schram D C and van de Sanden M C M 2001 *J. Appl. Phys.* **89** 2404
[52] Johnson N M, Walker J, Doland C M, Winer K and Street R A 1989 *Appl. Phys. Lett.* **54** 1872
[53] Oversluizen G and Lodders W H M 1998 *J. Appl. Phys.* **83** 8002
[54] Kessels W M M, van de Sanden M C M and Schram D C 1998 *J. Non-Cryst. Solids* **227–230** 133
[55] Lavareda G, Nunes de Carvalho C, Amaral A, Conde J P, Vieira M and Chu V 2002 *Vacuum* **64** 245
[56] Qiao J, Jiang Z and Ding Z 1985 *J. Non-Cryst. Solids* **77**, **78** 829
[57] Miyazaki K, Kajiwara T, Uchino K, Muraoka K, Okada T and Maeda M 1997 *J. Vac. Sci. Technol.* A **15** 149
[58] Tachibana K 1994 *Japan J. Appl. Phys.* **33** 4329
[59] Kessels W M M, Hoefnagels J P M, Boogaarts M G H, Schram D C and van de Sanden M C M 2001 *J. Vac. Sci. Technol.* A **19** 1027
[60] Agarwal S, Sriraman S, Takano A, van de Sanden M C M, Aydil E S and Maroudas D 2002 *Surf. Sci.* **515** L469
[61] Walch S P, Ramalingam S, Sriraman S, Aydil E S and Maroudas D 2001 *Chem. Phys. Lett.* **344** 249
[62] Widdra W, Yi S I, Maboudian R, Briggs G A D and Weinberg W H 1995 *Phys. Rev. Lett.* **74** 2074